Research Square

Preprints are preliminary reports that have not undergone peer review.
They should not be considered conclusive, used to inform clinical practice,
or referenced by the media as validated information.

Prolonged methionine restriction induces liver cancer persistence through RNA G-quadruplex-mediated translational inhibition of HNF4α

Xiaoling Li

lix3@niehs.nih.gov

National Institute of Environmental Health Sciences https://orcid.org/0000-0001-5920-7784

Qing Xu

National Institute of Environmental Health Sciences

Yi Fang

National Institute of Environmental Health Sciences

Igor Shats

National Institute of Environmental Health Sciences

Naiduwadura De Silva

Dinushi Gamagedara

Jian-Liang Li

National Institute of Environmental Health Sciences https://orcid.org/0000-0002-6487-081X

Jun Zhang

Article

Keywords: methionine restriction, translation, RNA G-quadruplex, SRSF1

Posted Date: September 21st, 2026

DOI: https://doi.org/10.21203/rs.3.rs-10167785/v1

License: This work is licensed under a Creative Commons Attribution 4.0 International License. Read Full License

Additional Declarations: There is **NO** conflict of interest to disclose.

Abstract

Methionine restriction, a dietary intervention that limits the intake of the essential amino acid methionine and imposes nutritional stress on cancer cells, has emerged as a potentially less toxic anti-cancer strategy. By cell-autonomously disrupting one-carbon metabolism, epigenetic regulation, and redox homeostasis, methionine restriction can inhibit tumor growth and enhance the sensitivity of certain human cancers to chemotherapy and radiotherapy in. However, because methionine is essential for normal cellular function, prolonged restriction may lead to adverse outcomes, including immune dysfunction, bone loss, and enhanced stress resistance. Consequently, the long-term influence of methionine restriction on cancer progression is complex and remains poorly understood. Here we report that prolonged methionine restriction in epithelial human liver cancer cells reduces translation of hepatocyte nuclear factor 4α (HNF4α), a master regulator of hepatocyte identity. The action leads to the formation of drug-tolerant persister cells that phenotypically resemble HNF4α-negative mesenchymal liver cancer cells. Mechanistically, we show that the 5′-untranslated region (5′-UTR) of the *HNF4A* mRNA harbors highly conserved RNA G-quadruplex (rG4) sequences recognized and bound by an RNA binding protein SRSF1, which facilitates HNF4α translation. Prolonged methionine restriction activates AMPK, reducing the binding of SRSF1 to *HNF4A* rG4 and attenuating HNF4α translation. Notably, overexpression of HNF4α from an rG4-free construct or inhibition of AMPK restores the sensitivity of established persisters to methionine restriction. Collectively, our findings uncover a post-transcriptional mechanism linking metabolic stress to remodeling of tumor cell identity and identify the AMPK-SRSF1-HNF4α axis as a potential therapeutic target for drug-resistant and metastatic liver cancer.

Introduction

Despite significant advances in cancer therapy, the development of treatment tolerance constitutes a major barrier to long-term clinical efficacy. Drug-tolerant persister cells (DTPs), a subpopulation of cancer cells capable of surviving initial treatment without acquiring permanent genetic resistance, play a pivotal role in tumor recurrence and metastasis [1–5]. The ability of DTPs to evade treatment-induced stress often requires the implementation of extended or more intensive therapeutic regimens. However, such approaches may paradoxically promote further tolerance while exacerbating treatment-related toxicity and adverse effects. Consequently, optimizing the duration and intensity of anticancer therapies remains a critical therapeutic challenge.

Methionine restriction is a dietary approach that restricts the intake of methionine, a sulfur-containing essential amino acid critical for protein synthesis, sulfur metabolism, epigenetic modification, antioxidant defense, and signaling [6]. This metabolic intervention has attracted considerable interest as an anti-cancer strategy, given its cell-autonomous capacity to rewire one-carbon metabolism, disrupt epigenetic regulation, and perturb redox homeostasis, thereby impairing tumor growth and enhancing therapeutic sensitivity [7–10]. Nevertheless, because methionine is indispensable for normal cellular physiology, prolonged restriction carries the risk of adverse effects, including bone loss and immune dysfunction [10–13]. Consequently, the long-term influence of methionine restriction on cancer progression is complex and remains poorly understood. Investigating how cancer cells adapt to prolonged methionine restriction is therefore critical for assessing its safety and therapeutic potential in clinical settings.

Liver cancer, one of the leading causes of cancer-related death, is notoriously resistant to conventional chemotherapy and radiotherapy. We previously reported that hepatocyte nuclear factor 4α (HNF4α), a master regulator of hepatic identity and liver-specific genes [14, 15], transcriptionally activates enzymes involved in the methionine cycle and transsulfuration pathway in epithelial human liver cancer cells [9]. This regulation suppresses epithelial-to-mesenchymal transition and confers sensitivity to methionine restriction [9]. In this study, we discover that some HNF4α-positive liver cancer cells can survive prolonged methionine restriction by acquiring traits typical of persistent cancer cells. Through genomic profiling, bioinformatic analysis, and molecular and cellular characterizations, we show that these persistent phenotypes result of translational inhibition of HNF4α, which is mediated by a pathway involving AMPK, RNA binding proteins and mRNA structural remodeling. Our findings demonstrate that translational reprogramming of HNF4α promotes adaptive persistence of liver cancer cells under sustained methionine restriction, revealing a previously unrecognized connection between energy stress signaling, RNA structure-dependent translational regulation, and adaptive cellular persistence.

Results

Epithelial human hepatocellular carcinoma (HCC) cells that survive prolonged methionine restriction display typical characteristics of persistent cancer cells

The commonly used dietary methionine restriction regimen restricts dietary methionine by 80% in the absence of cysteine [8, 16, 17]. To investigate the adaptive response of cancer cells to prolonged methionine restriction, we modified the cell culture medium by decreasing both methionine and cysteine concentrations from 200 μM each in complete DMEM medium (CM) to 10 μM each (MCR10 medium). We have previously shown that this concentration, which is slightly below the lower limit of the normal human plasma methionine range (13–45 μM) [18, 19], is able to suppress the growth of HNF4α-positive liver cancer cells such as HepG2 and Huh7 [9]. Consistent with these observations, both HepG2 and Huh7 cells markedly slowed down their growth upon switching into MCR10 medium (Figure S1A), while maintaining high viability after 48 hours of culture in this medium (Figure S1B). After 4 to 6 days, the remaining cells were extremely slow in proliferation compared to parental cells grown in CM (Fig. 1A) and displayed reduced protein synthesis, as indicated by decreased intensities of puromycin-labeled peptides in the SUnSET assay [20] (Fig. 1B). They also exhibited mesenchymal-like morphology (Fig. 1C) with an enhanced migration ability (Fig. 1D) and increased collagen deposition (Fig. 1E), all of which are suggestive of increased epithelial-mesenchymal transition (EMT). Consistently, the expression of *SNAI2*, a master regulator of EMT, along with several mesenchymal markers, such as *CDH2* and multiple collagen genes, was significantly increased in MCR10 surviving cells (Fig. 1F). Notably, MCR10 survivors were also resistant to the treatment with sorafenib (Fig. 1G), a first-line drug for advanced liver cancer that functions as an inhibitor to multiple kinases and the cysteine-glutamate antiporter (system x_c^-) [21, 22]. The slow proliferation, reduced protein synthesis, acquisition of mesenchymal features, and chemotherapy resistance exhibited by these MCR10 resistant cells are all hallmarks of persistent cancer cells [2–5, 23]. These residual, often clinically undetectable cancer cells can persist in the body following treatment and are key contributors to tumor relapse and metastasis [2–5, 23].

To better understand prolonged methionine restriction-induced persistence of liver cancer cells at the molecular level, we profiled the transcriptomes of MCR10 persisters derived from HepG2 and Huh7 cells, along with their respective parental cells cultured in CM by RNA-seq analysis. Compared to their parental counterparts, HepG2

MCR10 persisters showed significant changes in the expression of 2,690 genes, while Huh7 MCR10 persisters exhibited altered expression in 3,534 genes (Table S1, MCR10 persisters vs CM cells, |Fold change|≥2 and FDR < 0.05). Venn diagram analysis of these differentially expressed genes (DEGs) showed that among the total of 5,089 unique DEGs identified across both cell types, 451 were commonly induced while 556 were commonly reduced in MCR10 persisters derived from both HepG2 and Huh7 cells (Fig. 1H and Table S1). Further pathway analyses revealed that genes mediating cell migration, inflammation, and stress response were enriched in 451 commonly upregulated DEGs (Fig. 1I, MCR10_UP), whereas genes involved in cell cycle regulation, metabolism, detoxification, and translation were enriched in 556 commonly downregulated DEGs (Fig. 1I, MCR10_DOWN). These transcriptional changes aligned with the observed persister phenotypes.

The transcriptional signatures shared by both MCR10 persister populations were also relevant to the persister phenotypes reported in clinical cancer treatments. In a publicly available RNA-seq dataset of breast cancer samples collected before treatment, after two cycles of chemotherapy, and at final surgery following six cycles of chemotherapy [24], the expression of the MCR10_UP signature was significantly increased, while the MCR10_DOWN signature was significantly decreased in residual tumors (Fig. 1J). In a separate study of resectable rectal cancer [25], the expression of MCR10_DOWN signature was significantly reduced in residual tumors but not in normal tissues following preoperative radio-chemotherapy (RCT) (Figure S1C). Similarly, the expression of MCR10_DOWN signature was significantly decreased in residual resectable esophageal adenocarcinoma on combined neoadjuvant chemoradiotherapy and atezolizumab treatment [26] (Figure S1D). Together, our findings indicate that prolonged methionine restriction induces persistent liver cancer cells that exhibit characteristic morphological and molecular features of cancer persisters.

Prolonged methionine restriction reduces abundance of HNF4α protein in MCR10 persisters

The persister phenotypes of the MCR10-persistent liver cancer cells closely resembled those previously observed in liver cancer cells following HNF4α knockdown or in HNF4α-negative mesenchymal live cancer cells [9]. To understand how prolonged methionine restriction induces the persistence of liver cancer cells, we tested the hypothesis that the formation of persistent liver cancer cells is coupled with diminished HNF4α activity. In line with this possibility, in HepG2 cells, genes altered in MCR10 persisters (MCR10 vs CM) significantly overlapped with those changed by HNF4α knockdown (shHNF4α vs control, from a previously reported microarray dataset [27]) (Figure S2A and Table S2). Specifically, genes involved in stress response, apoptosis, and inflammation were significantly induced in both MCR10 persisters and HNF4α knockdown HepG2 cells, while genes involved in metabolism, inhibition of cell death, and cell adhesion were significantly suppressed in both conditions (Figure S2A). More strikingly, 218 out of the 556 downregulated genes shared by HepG2 and Huh7 persister cells have been previously identified as HNF4α target genes [28, 29] (Fig. 2A and Table S3), reinforcing the notion that formation of MCR10 persistent liver cancer cells is associated with reduced HNF4α transcriptional activity. Similar to the MCR10 signature genes, this subset of HNF4α target genes, involved in metabolism and cell division was also significantly decreased in residual tumors following clinical cancer treatment (Fig. 2B and S2B, MCR10_DOWN_ HNF4α signature).

In support of the notion that MCR10 persistent liver cancer cells had reduced HNF4α transcriptional activity, MCR10 persisters exhibited reduced levels of HNF4α protein compared to their parental cells cultured in CM (Fig. 2C), and this reduction was reversible as switching back to CM restored the HNF4α protein levels (Figure

S3A). Moreover, in HepG2 cells, the reduction of HNF4α protein was not coupled with reduced mRNA levels of *HNF4A* (Figure S3B), suggesting that MCR10 could directly decrease HNF4α protein. Indeed, during the four-day induction of MCR10 persisters from parental cells cultured in CM, the HNF4α protein levels were gradually reduced in both HepG2 and Huh7 cells (Fig. 2D). Furthermore, the reduction of HNF4α protein was accompanied with diminished HNF4α transcriptional activity, as the mRNA levels of various HNF4α target genes not directly associated with mesenchymal morphology were significantly decreased in MCR10 persisters (Fig. 2E). Intriguingly, the reduction in HNF4α protein was not unique to MCR10, as depletion of glutamine (a conditionally essential amino acid) or leucine (an essential amino acid) also led to decreased HNF4α protein levels (Fig. 2F), indicating that HNF4α protein is sensitive to general nutrient deprivation.

To directly test whether HNF4α reduction underlies MCR10-induced liver cancer persistence, we reintroduced WT or different mutant HNF4α proteins in MCR10 persisters (Figure S3C). Compared to the empty vector (Vector) and the GFP control, overexpression of WT HNF4α partially restored the sensitivity of the persisters to MCR10 treatment (Fig. 2G). In contrast, an HNF4α dominant negative mutant C106R [30], or a nonsense mutant lacking the E-domain required for normal HNF4α functions R154X [31], failed to rescue this sensitivity (Fig. 2G). Therefore, a functional HNF4α is required to overcome the resistance to MCR10 in persistent liver cancer cells. Together, our observations indicate that prolonged methionine restriction leads to the formation of persistent liver cancer cells by reducing HNF4α protein.

Prolonged methionine restriction decreases HNF4α protein through an RNA G-quardruplex-mediated translational inhibition

We then sought to understand how MCR10 reduces HNF4α protein levels. We first assessed the protein stability of HNF4α in both parental CM cells and MCR10 persisters using a cycloheximide (CHX) chase assay. However, despite the markedly reduced abundance of HNF4α protein in persisters, its degradation rate was comparable to that in the parental cells (Figure S3D). We next examined the synthesis of HNF4α protein by treating cells with MG132 to inhibit proteasomal degradation and then analyzing cellular HNF4α protein levels. This treatment resulted in a gradual accumulation of HNF4α protein in the parental cells, whereas no such increase was observed in MCR10 persisters (Fig. 3A), suggesting that HNF4α protein synthesis is impaired in MCR10 persister cells. In line with this finding, a ribosomal footprint assay revealed a marked increase in ribosome stalling at the translation initiation site (TIS) of *HNF4A* mRNA in MCR10 persisters (Fig. 3B, *HNF4A*). As a comparison, ribosome stalling at the TISs of *ATF4* and *ACTB* mRNAs was far less pronounced (Fig. 3B).

As an essential amino acid and the initiating amino acid in eukaryotic protein synthesis, methionine is crucial in translation. Specifically, translation initiation requires the assembly of the ternary complex of eukaryotic initiation factor 2 alpha (eIF2α), GTP, and the methionyl initiator tRNA (Met-tRNA) [32, 33]. Methionine restriction has been shown to impair this complex formation, thereby inhibiting the recognition of start codons and translation [34, 35]. Therefore, reduced HNF4α translation observed in MCR10 liver cancer persisters may reflect a global decrease in translation as we observed (Fig. 1B). However, we found that HNF4α protein expression from a mammalian expression construct lacking its endogenous untranslated regions (UTRs) was insensitive to MCR10 treatment (Figure S3E), suggesting that MCR10-induced translational suppression of endogenous HNF4α protein is mediated through its UTRs.

Bioinformatics analysis of UTRs of *HNF4A* mRNA revealed that its 5'-UTR harbored highly conserved RNA G-quadruplex (rG4)-forming sequences (Figure S3F). rG4s are four-stranded secondary structures formed by guanine-rich RNA sequences implicated in the control of mRNA translation, splicing, localization, and stability [36, 37]. We found that in both HepG2 and Huh7 cells, HNF4α was one of the top highly abundant transcription factors with high G4 scores (Fig. 3C, red). Interestingly, HNF1α and FOXA3, two additional transcription factors critical for hepatocyte identity, also had very high G4 scores (Fig. 3C, magenta and blue, respectively), suggesting that high rG4-forming sequences in 5'-UTR is a common feature of liver-enriched transcription factors.

rG4s have been recently shown to be stress-responsive cis-elements that dynamically fold into stable rG4 structures in response to cellular stress in human cells [38]. In particular, nutrient starvation can induce the folding of 72% rG4s in U2OS cells [39]. Therefore, as a nutrient restriction regimen, MCR10 may promote the folding of rG4s in the 5'-UTR of *HNF4A*, thereby inhibiting its translation. Indeed, MCR10 persisters displayed an increased G4 staining intensity, primarily in the cytosol when probed with a G4-specific antibody BG4 [40] (Fig. 3D). Notably, when the rG4 element of endogenous *HNF4A* was inserted in the 5'-UTR of the aforementioned mammalian *HNF4A* expression construct, the expression of HNF4α protein was dramatically diminished even in cells cultured in CM (Fig. 3E, G4-*HNF4A*), supporting the notion that this rG4 element strongly suppresses HNF4α translation in this CMV promoter-driven overexpression system.

Prolonged methionine restriction inhibits HNF4α protein translation by reducing SRSF1 binding to HNF4A rG4

To identify factors that enable endogenous HNF4α translation under the CM condition despite the strong translational inhibition imposed by its 5'-UTR rG4, we analyzed the potential RNA binding proteins (RBPs) interaction sites within this region using RBPmap [41]. Among the top candidate RBPs identified, Heterogeneous nuclear ribonucleoprotein H2 (HNRNPH2) and Serine and Arginine Rich Splicing Factor 1 (SRSF1) exhibited high predicted binding scores across multiple sites within this region (Fig. 4A and S3F). Although both RBPs have been reported to bind and unwind rG4 structure [42, 43], our RNA-seq data showed that HNRNPH2 was not detectable in HepG2 or Huh7 cells (Figure S4A). We therefore focused our subsequent analysis on SRSF1.

Previously known as SF2/ASF, SRSF1 is a member of the serine/arginine-rich family of RNA-binding proteins that primarily regulate pre-mRNA splicing [11, 44]. It is a 248-residue protein containing two N-terminal RNA-Recognition Motifs (RRMs) and a C-terminal RS domain enriched in repetitive Arg/Ser dipeptides (Fig. 4B) [11]. The two RRMs mediate the sequence-specific RNA binding, and the RS domain promotes protein-protein interaction. SRSF1 also continuously shuttles between the nucleus and cytoplasm, a process that depends on the RS domain [45, 46]. Consequently, in addition to its role in splicing, SRSF1 participates in multiple post-splicing processes, including mRNA nuclear export, nonsense-mediated mRNA decay, and mRNA translation [47, 48]. We confirmed that the SRSF1 RNA binding domain (RBD) containing two RRMs could directly bind the rG4 element of *HNF4A* in an in vitro binding assay, with a Kd around 500 nM (Fig. 4C). In MCR10 persisters derived from both HepG2 and Huh7 cells, the mRNA abundance of *SRSF1* was significantly reduced (Figure S4A and S4B), whereas its protein levels remained unchanged (Figure S4C). RBP immunoprecipitation (RIP) assays revealed that SRSF1 strongly bound to the 5'-UTR of *HNF4A* mRNA in parental cells cultured in CM (Fig. 4D, CM, SRSF1 vs IgG). In MCR10 persisters, this binding was significantly reduced despite the normal SRSF1 protein abundance (Fig. 4D, MCR10 vs CM), suggesting that MCR10-induced alterations in SRSF1 protein and/or rG4 interfere with their interaction. Moreover, overexpression of SRSF1 dose-dependently increased the translation of HNF4α protein from the rG4-containing construct in cells cultured in CM (Fig. 4E and S4D). All these observations

strongly suggest that the reduced binding of SRSF1 to *HNF4A* rG4 in MCR10 persisters is responsible for diminished HNF4α translation.

In agreement with this possibility, siRNA-mediated knockdown of SRSF1 in parental liver cancer cells decreased the HNF4α protein expression (Fig. 4F and 4G) and induced a mesenchymal morphology in cells cultured in CM (Fig. 4H). Moreover, the mRNA levels of HNF4α target genes were reduced, whereas those of EMT-related genes were elevated in SRSF1 knockdown cells (Fig. 4I). Taken together, our results indicate that MCR10 reduces the binding of SRSF1 to the rG4 structure in the 5′UTR of *HNF4A* mRNA, thereby inhibiting HNF4α protein translation and inducing persister formation.

Activation of AMPK partially underlies persister formation induced by prolonged methionine restriction

The binding of SRSF1 to RNA is regulated by multiple mechanisms, particularly posttranslational modifications. For instance, SRSF1 is methylated at R93, R97, and R109, a linker region between the two RRMs important for the sequence-specific RNA-binding (Fig. 4B) [49]. These modifications have previously been shown to be important for the proper subcellular localization of SRSF1 and its ability to bind mRNA and proteins, and are therefore critical for alternative splicing [50–52]. Moreover, many Ser residues in the RS domain of SRSF1 are phosphorylated, and the transitions between hypophosphorylation and hyperphosphorylation directly influence its protein interaction, RNA-binding, and subcellular localization [53].

To understand how prolonged methionine restriction reduces the binding of SRSF1 to *HNF4A* rG4, we first investigated the possible contribution of SRSF1 arginine methylation, as methionine restriction is known to decrease intracellular levels of the major cellular methyl-donor S-adenosylmethionine (SAM) and impair protein methylation [9, 54]. However, immunofluorescence imaging revealed no significant change in the subcellular localization of endogenous SRSF1 in MCR10 persisters compared with parental cells cultured in CM (Figure S5A). Moreover, mutation of R93, R97, and R109 to either lysine (R3K) or alanine (R3A) dramatically reduced the expression SRSF1 in both HepG2 and Huh7 cells (Figure S5B), preventing us from evaluating the impact of SRSF1 arginine methylation on HNF4α translation.

We then screened several small-molecule metabolites and pharmacological compounds associated with methionine or nutrient restriction to determine whether any could mimic MCR10-mediated reduction of HNF4α protein in parental CM cells or restore HNF4α expression in MCR persisters. The compounds tested included AICAR, an AMP mimetic that activates AMP-activated protein kinase (AMPK), a serine/threonine kinase that serves as a central energy and stress sensor [55, 56]; glutathione (GSH), GYY4137 (GYY), and N-acetyl-cysteine (NAC), three sulfur-containing metabolites directly linked to the transsulfuration pathway and glutathione synthesis downstream of the methionine cycle that are important to protect against methionine restriction-induced EMT [9]; and GO6983, a broad-spectrum inhibitor of protein kinase C (PKC). The latter was included based on evidence that activation of PKC by various stress signals promotes HNF4α phosphorylation and subsequent proteasome-mediated degradation [57–59]. Intriguingly, of all compounds tested, only AICAR reduced HNF4α protein in CM cells, with no additive effect observed in MCR10 persisters (Fig. 5A). This finding suggests that prolonged methionine restriction may suppress HNF4α translation, at least in part, by activating AMPK. We confirmed that prolonged methionine restriction increased AMPK phosphorylation, similar to the effect of AICAR treatment (Fig. 5B and 5C). AMPK has been previously reported to directly phosphorylate SRSF1

at Ser133 within the RRM2 domain (Fig. 4B), which in turn suppresses the interaction between SRSF1 and specific RNA sequences without altering the subcellular localization of SRSF1 [60]. Therefore, it is possible that AMPK-induced phosphorylation of SRSF1 at S133 impairs its binding with *HNF4A* rG4 upon MCR10 in liver cancer cells, thereby contributing to translational suppression of HNF4α. Consistent with this notion, the SRSF1 RBD S133E mutant, which mimics S133 phosphorylation, displayed an approximately 3.6-fold reduction in binding affinity toward the *HNF4A* rG4 element in vitro (Fig. 5D, compared to Fig. 4C). Again, we were unable to assess the impact of SRSF1 S133 phosphorylation on HNF4α translation in cells because neither the phosphorylation-mimetic mutants (S133E and S133D) nor the dephosphorylation-mimetic mutant (S133A) were stable in HepG2 and Huh7 cells (Figure S5C). Nevertheless, we observed that AICAR-induced reduction of HNF4α protein was partially rescued by SRSF1 overexpression (Fig. 5E).

AICAR treatment not only recapitulated the effect of MCR10 on HNF4α protein expression (Fig. 5A and 6A), but also induced similar mesenchymal-like morphological and molecular features (Fig. 6B and 6C). Notably, AICAR-treated cells became resistant to MCR10-induced inhibition of cell proliferation (Fig. 6D), whereas MCR10 presisters were sensitive to AMPK inhibition by Compound C (Fig. 6E). Collectively, our findings support a model in which prolonged methionine restriction activates AMPK, leading to SRSF1 phosphorylation and reduced binding to the *HNF4A* rG4 element, thereby suppressing HNF4α protein translation and promoting persister formation (Fig. 6F).

Discussion

Dietary methionine restriction has been shown to extend life span, reduce adiposity, and improve insulin sensitivity through various signaling pathways in preclinical animal models [16, 17, 61–64]. More recently, methionine restriction has emerged as a promising dietary intervention capable of inducing rapid and tumor-selective metabolic reprogramming to enhance cancer therapeutic outcomes, particularly in advanced-stage disease[8–10]. In this study, however, we uncover an unexpected adaptive response to prolonged methionine restriction in HCC, whereby chronic nutrient stress promotes a drug-tolerant persister phenotype through translational suppression of HNF4α. Mechanistically, we show that AMPK activation under methionine restriction disrupts SRSF1 interaction with rG4 structures within the *HNF4A* 5'UTR, resulting in reduced HNF4α translation. These findings reveal a previously unrecognized link between metabolic stress signaling, RNA structure-dependent translational regulation, and cancer cell persistence.

Our results contribute to growing body of evidence that metabolic interventions can exert both anti-proliferative and adaptive effects in tumor cells. While methionine restriction has been shown to inhibit tumor growth and sensitize tumors to chemotherapy and radiotherapy [7–9], we propose that chronic nutrient limitation may also impose selective pressure favoring survival of stress-adapted cell populations (Fig. 1). The persister-like state observed here is consistent with previous studies demonstrating that non-genetic cellular plasticity contributes to therapeutic resistance across multiple cancer types [1–5]. In this context, our findings suggest that prolonged methionine restriction may promote survival programs that allow a subset of cells to tolerate unfavorable conditions without acquiring stable genetic alterations, which has important implications for the durability of dietary interventions as anticancer strategies.

A central finding of our study is the identification of HNF4α translational repression as a mediator of this adaptive response (Fig. 2). HNF4α is a key regulator of hepatocyte differentiation and liver-specific transcriptional programs [14, 15]. Reduced HNF4α expression has been associated with aggressive HCC

phenotypes [65–67]. We have previously shown that epithelial liver cancer cells expressing high levels of HNF4α are sensitive to methionine restriction [9]. Our data in the present study suggest that metabolic stress can modulate hepatocyte identity and stress sensitivity through post-transcriptional mechanisms, expanding current understanding of how nutrient availability shapes tumor cell state. Whether HNF4α suppression is sufficient to fully drive persistence or instead acts as part of a broader adaptive network remains an important question for further investigation.

Our work also establishes a functional role for rG4-mediated translational control in metabolic stress adaptation (Figs. 3 and 4). Many liver-enriched transcription factors have rG4 elements in the 5'-UTR (Fig. 3C) [68] and the folding of these elements into stable rG4 structures have been reported to be sensitive to stress, particularly nutrient starvation [38, 39]. However, the contribution of these structures to cancer adaptation remains largely unknown. Our finding that SRSF1 binding to *HNF4A* rG4 motifs is sensitive to AMPK signaling (Figs. 5 and 6) suggests that RNA structural elements may serve as dynamic interfaces between metabolic signaling and translational regulation. It will be important in future studies to determine whether additional stress-responsive transcripts are regulated through similar mechanisms.

Our study has several limitations. First, the methionine restriction conditions used in the present study may not fully recapitulate the degree or chronicity of dietary methionine restriction achievable in clinical settings. Second, while the present study is focused on HCC, whether this adaptive mechanism operates in other tumor types with distinct metabolic dependencies remains to be established. Third, HNF4α is unlikely to be the sole translationally regulated effector of methionine restriction, and systematic identification of additional targets will be necessary to fully characterize the scope of this adaptive response. Finally, the long-term in vivo consequences of methionine-induced persistence, including potential effects on tumor recurrence and metastasis, remain to be determined.

In summary, our study identifies an AMPK–SRSF1–rG4 signaling axis that mechanistically links methionine restriction to translational suppression of HNF4α and the emergence of a persister-like state in HCC. These findings provide insight into how metabolic stress remodels tumor cell identity through post-transcriptional regulation and highlight the importance of considering adaptive resistance mechanisms when developing metabolic therapeutic strategies.

Methods

Cell culture

HCC cell lines HepG2 and Huh7 were purchased from ATCC and maintained in complete DMEM medium (CM) containing 200 μM of methionine and cysteine each, supplemented with 10% FBS (Hyclone). To induce persisters, the parental HepG2 and Huh7 cells were switched to an MCR10 medium (MCR10) containing 10 μM of methionine and cysteine each and cultured for 4 to 6 days.

To knock down SRSF1 gene, siRNAs against SRSF1 (Thermo Fisher Scientific, S12725), and a negative siRNA (siNeg, 4390843) were purchased from ThermoFisher Scientific and transfected into liver cancer cells with Lipofectamine RNAiMAX (ThermoFisher Scientific).

Overexpression Plasmids

pcDNA3-HNF4A, the cDNA ORF clones of HNF4α (OHu25290D, NCBI Reference Sequence: NM_000457.6), was purchased from Genscript USA. QuikChange II Site-Directed Mutagenesis Kit was used to create the HNF4α dominant negative mutant C106R, nonsense mutant R156X lacking the E-domain required for normal HNF4α functions. To create G4-*HNF4A* expression plasmid, GenBuilder™ Cloning Kit (Genscript) was used to insert the sequence for the 5'UTR of *HNF4A* "GGGAGGAGGCAGTGGGAGGGCGGAGGGCGGGGGCCTTCGGGGTGGGCGCCCAGGGTAGGGCAGGTGGCCGCGGCGTGGAGGCAGGGAGA" immediately upstream of the translation start site of the *HNF4A* cDNA in the plasmid pcDNA-HNF4a plasmid.

Cell survival assays

CyQUANT™ Direct Cell Proliferation Assay (Thermo Fisher Scientific) were used to measure the response of HepG2 and Huh7 cells to MCR10 restriction or sorafenib treatment.

Crystal violet staining was used to measure the effect of overexpression of HNF4α on the cell survival in MCR10 restriction. After transfection with the plasmids in 12-well plates, the persistent cells were cultured in the MCR10 medium for another 24 h. The medium was then removed, and the cells were washed with DPBS and stained with 0.1% Crystal violet solution (Sigma) for 15 min at RT. The wells were rinsed with water and air dried overnight. The dye was then eluted with methanol, and the OD was measured at 540 nM.

Collagen staining

The staining was performed according to a protocol described in Trackman et al [69]. The cells were fixed with Bouin's solution for 10 min and stained with Sirius red dye solution for 1 h at RT. After staining, the cells were washed with 0.5% glacial acetic acid. The bound dye was eluted with 0.1 M NaOH and the OD was measured at 550 nm. Cell density in each well were measured with Crystal violet staining as described in the section of cell survival assays. Data is expressed as the ratio of total absorbance of Sirius red/Crystal violet.

Immunoblotting

Protein samples were separated by SDS-PAGE, transferred to PVDF membrane, and blotted with following antibodies: HNF4α (Santa Cruz, sc-374229), FLAG (Sigma, F1804-50UG), SRSF1 (SF2/ASF, Santa Cruz, sc-33652). All antibodies used in this study are included in Table S4.

Cell migration assay

To analyze the cell migration ability, Cells cultured in CM or MCR10 medium were trypsinized and plated with serum-free DMEM on the top of the membrane in a transwell insert with 8 μM pore size (Corning). The inserts were placed in the wells of a 24-well plate filled with 10% FBS-containing DMEM, cultured for 24 hours and then stained with crystal violet (Sigma). A cotton-tipped applicator was used to remove the non-migrated cells on the top side of the insert. Migrated cells were imaged with a microscope and quantified with the ImageJ 2.0.0 (Fiji) software.

RNA isolation, quantitative real-time PCR and RNA-seq

Total RNA was purified from cells using RNeasy Mini kit (Qiagen). For quantitative real time PCR analysis, RNA was reverse transcribed using High-Capacity cDNA Reverse Transcription kit (Thermo Fisher Scientific). Real-time PCR assays were conducted on a CFX96 or CFX Opus 384 real-time PCR instruments (Bio-Rad) utilizing iQ SYBR Green SuperMix (Bio-Rad). Primer sequences can be found in Table S5.

To conduct RNA-seq analysis, libraries were prepared using the TruSeq Stranded Total RNA kit (Illumina, San Diego, CA) with Ribo-Zero technology. Indexed samples were sequenced on a Nova-seq 6000 (Illumina) using a 75-bp single-end protocol according to the manufacturer's instructions. Raw sequencing data were trimmed to remove adaptors and poor-quality reads (average quality score less than 20) using Trim-galore (version 0.6.10). Cleaned reads were aligned to the human reference genome (hg38) using the STAR aligner (version 2.6.c) [70]. Ambiguous mapped reads and reads with a MAPQ score less than 10 were removed. Gene quantification was performed using Subread featureCounts (version 2.0.1) [71] with the hg38 NCBI RefSeq gene annotation. Genes with zero read counts across all samples were excluded from further analysis. Principal Component Analysis (PCA) and hierarchical clustering were applied to identify potential sample outliers. Differential gene expression analysis between control and treatment groups were conducted using the edgeR package (version 3.32.1). False discovery rate (FDR) correction was performed using the Benjamini and Hochberg method. Genes were considered significantly differentially expressed if they met the following criteria: detected in at least one sample (RPKM > 1), fold change over 2, and adjusted p-value less than 0.05. The heatmaps were generated using gplots R package.

Pathway Enrichment Analysis

All pathway enrichment analysis were preformed using generated differential gene lists in https://biit.cs.ut.ee/gprofiler/gost.

Analysis of MCR10 and HNF4α signatures in clinical datasets

The MCR10_UP signature consisted of 451 genes significantly (Fold change≥2 and FDR-adjusted $p < 0.05$) upregulated in both HepG2 and Huh7 persister cells grown in MCR10 medium compared with their corresponding parental lines grown in complete medium (CM). The MCR10_DOWN signature consisted of 556 genes significantly (Fold change < 0.5 and FDR-adjusted $p < 0.05$) downregulated in both HepG2 and Huh7 persister cells grown in MCR10 medium compared with their corresponding parental lines grown in complete medium (CM). The MCR10_DOWN_HNF4α signature of 218 genes consisted of a subset of the MCR10_DOWN signature previously identified as HNF4α target genes [28, 29] (https://maayanlab.cloud/Harmonizome/gene_set/HNF4A/CHEA+Transcription+Factor+Targets). All signatures can be found in Table S1 and S3.

The publicly available gene expression datasets of breast cancer samples collected before treatment, after two cycles of chemotherapy, and at final surgery following six cycles of chemotherapy (GSE87455) [24], resectable rectal cancer before and after preoperative radio-chemotherapy (GSE15781)[25], and resectable esophageal adenocarcinoma before and after combined neoadjuvant chemoradiotherapy and atezolizumab treatment (GSE165252) [26] were downloaded from GEO. Expression of genes comprising each signature was extracted and their averages was used as a measure of the corresponding signature expression in each sample.

Immunofluorescence

Cells on coverslips in 12-well plates were fixed with 4% formalin at room temperature for 10 min, washed with DPBS, permeabilized with 0.25% Triton X-100 for 10 min, and blocked with 1% BSA in PBST for 1 hour. Cells were then incubated with BG4 primary antibody for 1 hour followed by anti-Mouse IgG Alexa Fluor™ 488 (Thermo Fisher) for 1 hour at room temperature. Coverslips were mounted with VECTASHIELD HardSet Mounting Medium with DAPI (Vector Laboratories) and imaged using a confocal microscope.

Targeted ribosomal footprinting

Targeted ribosomal footprinting was performed as previously described in Li et al. Cells were lysed in buffer containing 20 mM Tris (pH 7.4), 150 mM NaCl, 5 mM $MgCl_2$, 1 mM DTT, 1 mg/mL cycloheximide, and 1% Triton X-100. Lysates were centrifuged at 20,000 × g for 5 min at 4°C, and the RNA-containing supernatant was collected. RNA concentration was quantified using the Qubit RNA HS assay. Equal amounts of RNA from each sample were treated with 1,000 U RNase I (Invitrogen) to generate ribosomal footprints and 10 U Turbo DNase (Invitrogen) to remove genomic DNA. Ribosomal footprints were extracted using TRIzol followed by isopropanol precipitation. Reverse transcription was performed using SuperScript III reverse transcriptase and footprint-specific primers targeting the region surrounding the translation initiation site, which contained added sequences for a common reverse primer. The RT was programed with a ramped temperature from 40°C to 50°C over 1 h. The RNA template was subsequently hydrolyzed with NaOH. cDNA purified by isopropanol precipitation was then used for qPCR with iQ SYBR Green Supermix (Bio-Rad) using a ribosome footprint–specific forward primer targeting the translation initiation site and a common reverse primer.

Binding of SRSF1 RBD to the 5'UTR of HNF4A in in vitro

SRSF1 RRM tandem (residues 1-196) and its S133E mutant were expressed and purified using the previously reported protocol [43, 72]. Briefly, transformed BL21-CodonPlus (DE3) cells were cultured to an OD600 of 0.6, followed by overnight protein expression induced by 0.5 mM IPTG at 22°C. Cell pellets were suspended in 20 mM Tris – HCl, pH 7.5, 150 mM Arg/Glu 2 M NaCl, 25 mM imidazole, 0.2 mM TCEP, 1 mM PMSF, 0.5 mg/mL lysozyme, and 1 tablet of protease inhibitor. Cell lysate was loaded to 5 ml of Ni-NTA resin, washed, eluted, and followed by Ulp1 cleavage to remove SUMO. Then the sample was diluted by threefold with 20 mM MES, pH 4.6, 100 mM Arg/Glu, and 0.1 mM TCEP before loading onto a 5-mL HiTrap Heparin column. The sample was eluted over a gradient with 20 mM MES, pH 11.5, 400 mM Arg/ Glu, 0.1 mM TCEP, 2 M NaCl, and 0.02% NaN_3. Fractions containing SRSF1 were pooled, and pH was adjusted to 6.0–8.0 followed by concentration. The sample was exchanged to a buffer containing 20mM Tris-HCl pH 7.5, 0.4 M Arg/Glu, and 0.2 mM TCEP.

HNF4α RNA G-quadruplex (sequence: AGGGAGGGCGGAGGGCGGG) was a synthetic product of IDT with 6-FAM at the 5' end and used directly. Ten μM of RNA was dissolved in 20 mM Tris-HCl, pH 7.5, 25 mM KCl, and 0.1 mM EDTA, and folded using a thermocycler by heating the RNA at 95˚C for 5 min, followed by an annealing gradient to 4˚C at a rate of 1 ˚C per minute. Folding of G-quadruplex was verified by circular dichroism.

Fluorescence polarization assays were performed in 25 mM KCl, 0.25 M Arg/Glu, 20 mM Tris-HCl pH 7.5, 0.1 mM EDTA, 0.1 mM TCEP, and 0.02% TWEEN 20. Ten nM of 5' fluorescein-labeled RNA was mixed with proteins at varying concentrations in black flat-bottom 96-well plates (Costar). Protein-RNA mixtures (50 μL) were mixed at 100 RPM for 10 min, followed by incubation at 37 ^{o}C for 30 min, and then at 25 ^{o}C for 10 min. Fluorescence polarization measurements were carried out using a Cytation 5 with an excitation wavelength of 485 nm and an emission wavelength of 520 nm. We have shown that the total fluorescence intensities did not change during

protein titration. Therefore, the dissociation constants (K_D) were fitted using the quadratic equation with assumption of one-site interaction. The fluorescence polarization (Fp) binding curves were fitted using the quadratic equation below, where the fitting parameters F_{min}, F_{max}, and K_D represent the fluorescence polarization baseline, plateau, and dissociation constant, respectively. [P_T] represents the total protein concentration, and [L_T] represents the total RNA concentration (10 nM). Errors in dissociation constants were calculated based on three independent measurements.

$$F_p = F_{min} + (F_{max} - F_{min}) \frac{\left[([P_T] + [L_T] + K_D) - (([P_T] + [L_T] + K_D)^2 - 4[P_T][L_T])^{0.5}\right]}{2[L_T]}$$

Binding of SRSF1 to the 5'UTR of HNF4A in cells

The RNA immunoprecipitation was performed based on the methods described in Surani et al. and Luige et al. [73, 74]. Cells were lysed with RIP lysis buffer containing Pierce IP Lysis Buffer 87787, 20 U/ml Rnase inhibitor (Rnasin, Promega), 1.0 mM DTT, and 1Xproteinase/phosphtase inhibitor. After incubation on ice for 10 min, the lysates were centrifuged at 14,000 × g at 4 degrees for 15 min. 1% of lysate was saved for input analysis. The lysates were precleared with Protein G Dynabeads and then incubated with Protein G Dynabeads bound with either SRSF1 antibody or the anti-mouse control IgG for 6h. The beads were then washed 5X with the RIP buffer and resuspended in 100 ul nuclease-free water. RNA bound to the protein was released after incubation at 65C for 15 min and then treated with DNase I at 37C for 15 min. RNA was then extracted with Trizol and reverse-transcribed to cDNA for qPCR.

Quantification and statistical analysis

Values are expressed as mean ± standard error of mean (SEM) from at least three independent experiments or biological replicates, unless otherwise indicated in the figure legend. Significant differences between the means were analyzed by the two-tailed, unpaired, Student's t-test, and differences were considered significant at $p < 0.05$. Differences between the means with more than two comparison groups were analyzed by Brown-Forsythe and Welch ANOVA test or two-way ANOVA with correction for multiple comparisons by controlling the false discovery rate and adjusted p-values (q-values) were reported. Data were analyzed using Prism Software 7.0 (GraphPad) or Microsoft Office Excel (Version 16.10).

Declarations

Data availability

The RNA-seq dataset of this study have been deposited to Gene Expression Omnibus under the number GSE314964:

https://www.ncbi.nlm.nih.gov/geo/query/acc.cgi?acc=GSE314964

Token *adopguecphivpix*.

Competing interests

Authors declare no competing interests.

Author contributions

Q. X. designed the study, performed experiments, analyzed data, and wrote the manuscript; Y. F. analyzed data, designed experiments, and performed the immunofluorescence staining experiments; I. S. analyzed clinical RNA-seq datasets. N. I. U. D., D. G., and J. Z. analyzed the binding of WT and S133E mutant SRSF1 RBD to *HNF4A* rG4 in vitro; J. L. analyzed the RNA-seq dataset; X. L. guided, designed, and coordinated the study, analyzed data, and wrote the manuscript. All authors critically reviewed the manuscript.

Acknowledgements

We thank the Li laboratory for critical reading of the manuscript; NIEHS Fluorescence Microscopy and Imaging Center for help with immunofluorescent analyses; NIEHS Epigenomics Core for RNA sequencing. This research was supported by the Intramural Research Program of National Institute of Environmental Health Sciences of the National Institutes of Health Z01 ES102205 (to X. L.). N. I. U. D. S., D. G., and J. Z. were supported by the National Institutes of Health R35GM147091 (to J. Z.).

The contributions of the NIH authors were made as part of their official duties as NIH federal employees, are in compliance with agency policy requirements, and are considered Works of the United States Government. However, the findings and conclusions presented in this paper are those of the authors and do not necessarily reflect the views of the NIH or the U.S. Department of Health and Human Services.

References

1. Sharma SV, Lee DY, Li B, Quinlan MP, Takahashi F, Maheswaran S *et al*. A chromatin-mediated reversible drug-tolerant state in cancer cell subpopulations. *Cell* 2010; 141: 69–80.
2. Shen S, Vagner S, Robert C. Persistent Cancer Cells: The Deadly Survivors. *Cell* 2020; 183: 860–874.
3. Bell CC, Gilan O. Principles and mechanisms of non-genetic resistance in cancer. *Br J Cancer* 2020; 122: 465–472.
4. Marine JC, Dawson SJ, Dawson MA. Non-genetic mechanisms of therapeutic resistance in cancer. *Nat Rev Cancer* 2020; 20: 743–756.
5. Sun X, Wu LF, Altschuler SJ, Hata AN. Targeting therapy-persistent residual disease. *Nat Cancer* 2024; 5: 1298–1304.
6. Mato JM, Martinez-Chantar ML, Lu SC. Methionine metabolism and liver disease. *Annu Rev Nutr* 2008; 28: 273–293.
7. Sanderson SM, Gao X, Dai Z, Locasale JW. Methionine metabolism in health and cancer: a nexus of diet and precision medicine. *Nat Rev Cancer* 2019; 19: 625–637.
8. Gao X, Sanderson SM, Dai Z, Reid MA, Cooper DE, Lu M *et al*. Dietary methionine influences therapy in mouse cancer models and alters human metabolism. *Nature* 2019; 572: 397–401.
9. Xu Q, Li Y, Gao X, Kang K, Williams JG, Tong L *et al*. HNF4alpha regulates sulfur amino acid metabolism and confers sensitivity to methionine restriction in liver cancer. *Nat Commun* 2020; 11: 3978.

10. Ji M, Xu Q, Li XL. Dietary methionine restriction in cancer development and antitumor immunity. *Trends Endocrin Met* 2024; 35: 400–412.
11. Manley JL, Krainer AR. A rational nomenclature for serine/arginine-rich protein splicing factors (SR proteins). *Gene Dev* 2010; 24: 1073–1074.
12. Huang TH, Lewis JL, Lin HS, Kuo LT, Mao SW, Tai YS *et al*. A Methionine-Restricted Diet and Endurance Exercise Decrease Bone Mass and Extrinsic Strength but Increase Intrinsic Strength in Growing Male Rats. *J Nutr* 2014; 144: 621–630.
13. Ji M, Xu X, Xu Q, Hsiao YC, Martin C, Ukraintseva S *et al*. Methionine restriction-induced sulfur deficiency impairs antitumour immunity partially through gut microbiota. *Nat Metab* 2023; 5: 1526–1543.
14. Sladek FM, Zhong WM, Lai E, Darnell JE, Jr. Liver-enriched transcription factor HNF-4 is a novel member of the steroid hormone receptor superfamily. *Genes Dev* 1990; 4: 2353–2365.
15. Sladek FM, Seidel SD. Hepatocyte Nuclear Factor 4α. *Nuclear Receptors and Genetic Diseases* 2001: 309–361.
16. Orentreich N, Matias JR, DeFelice A, Zimmerman JA. Low methionine ingestion by rats extends life span. *J Nutr* 1993; 123: 269–274.
17. Miller RA, Buehner G, Chang Y, Harper JM, Sigler R, Smith-Wheelock M. Methionine-deficient diet extends mouse lifespan, slows immune and lens aging, alters glucose, T4, IGF-I and insulin levels, and increases hepatocyte MIF levels and stress resistance. *Aging Cell* 2005; 4: 119–125.
18. Nimni ME, Han B, Cordoba F. Are we getting enough sulfur in our diet? *Nutr Metab (Lond)* 2007; 4: 24.
19. Navik U, Sheth VG, Khurana A, Jawalekar SS, Allawadhi P, Gaddam RR *et al*. Methionine as a double-edged sword in health and disease: Current perspective and future challenges. *Ageing Res Rev* 2021; 72: 101500.
20. Schmidt EK, Clavarino G, Ceppi M, Pierre P. SUnSET, a nonradioactive method to monitor protein synthesis. *Nat Methods* 2009; 6: 275–277.
21. Dixon SJ, Patel DN, Welsch M, Skouta R, Lee ED, Hayano M *et al*. Pharmacological inhibition of cystine-glutamate exchange induces endoplasmic reticulum stress and ferroptosis. *Elife* 2014; 3: e02523.
22. Yang WS, Stockwell BR. Ferroptosis: Death by Lipid Peroxidation. *Trends Cell Biol* 2016; 26: 165–176.
23. He J, Qiu Z, Fan J, Xie X, Sheng Q, Sui X. Drug tolerant persister cell plasticity in cancer: A revolutionary strategy for more effective anticancer therapies. *Signal Transduct Target Ther* 2024; 9: 209.
24. Kimbung S, Markholm I, Bjohle J, Lekberg T, von Wachenfeldt A, Azavedo E *et al*. Assessment of early response biomarkers in relation to long-term survival in patients with HER2-negative breast cancer receiving neoadjuvant chemotherapy plus bevacizumab: Results from the Phase II PROMIX trial. *Int J Cancer* 2018; 142: 618–628.
25. Snipstad K, Fenton CG, Kjaeve J, Cui G, Anderssen E, Paulssen RH. New specific molecular targets for radio-chemotherapy of rectal cancer. *Mol Oncol* 2010; 4: 52–64.
26. van den Ende T, de Clercq NC, van Berge Henegouwen MI, Gisbertz SS, Geijsen ED, Verhoeven RHA *et al*. Neoadjuvant Chemoradiotherapy Combined with Atezolizumab for Resectable Esophageal Adenocarcinoma: A Single-arm Phase II Feasibility Trial (PERFECT). *Clin Cancer Res* 2021; 27: 3351–3359.
27. Wang Z, Bishop EP, Burke PA. Expression profile analysis of the inflammatory response regulated by hepatocyte nuclear factor 4alpha. *BMC Genomics* 2011; 12: 128.

28. Diamant I, Clarke DJB, Evangelista JE, Lingam N, Ma'ayan A. Harmonizome 3.0: integrated knowledge about genes and proteins from diverse multi-omics resources. *Nucleic Acids Res* 2025; 53: D1016–D1028.
29. Rouillard AD, Gundersen GW, Fernandez NF, Wang Z, Monteiro CD, McDermott MG *et al*. The harmonizome: a collection of processed datasets gathered to serve and mine knowledge about genes and proteins. *Database (Oxford)* 2016; 2016.
30. Taylor DG, Haubenwallner S, Leff T. Characterization of a dominant negative mutant form of the HNF-4 orphan receptor. *Nucleic Acids Res* 1996; 24: 2930–2935.
31. Lindner T, Gragnoli C, Furuta H, Cockburn BN, Petzold C, Rietzsch H *et al*. Hepatic function in a family with a nonsense mutation (R154X) in the hepatocyte nuclear factor-4alpha/MODY1 gene. *J Clin Invest* 1997; 100: 1400–1405.
32. Hershey JWB, Merrick WC. Pathway and mechanism of initiation of protein synthesis. In: Sonenberg N, Hershey, J. W. B. & Mathews, M. B. (ed). *Translational Control of Gene Expression* Cold Spring Harbor Laboratory Press: Cold Spring Harbor, NY, 2000, pp 33–38.
33. Kapp LD, Lorsch JR. GTP-dependent recognition of the methionine moiety on initiator tRNA by translation factor eIF2. *J Mol Biol* 2004; 335: 923–936.
34. Stone KP, Ghosh S, Kovalik JP, Orgeron M, Wanders D, Sims LC *et al*. The acute transcriptional responses to dietary methionine restriction are triggered by inhibition of ternary complex formation and linked to Erk1/2, mTOR, and ATF4. *Sci Rep* 2021; 11: 3765.
35. Mazor KM, Dong L, Mao Y, Swanda RV, Qian SB, Stipanuk MH. Effects of single amino acid deficiency on mRNA translation are markedly different for methionine versus leucine. *Sci Rep* 2018; 8: 8076.
36. Kharel P, Becker G, Tsvetkov V, Ivanov P. Properties and biological impact of RNA G-quadruplexes: from order to turmoil and back. *Nucleic Acids Res* 2020; 48: 12534–12555.
37. Dumas L, Herviou P, Dassi E, Cammas A, Millevoi S. G-Quadruplexes in RNA Biology: Recent Advances and Future Directions. *Trends Biochem Sci* 2021; 46: 270–283.
38. Kharel P, Ivanov P. RNA G-quadruplexes and stress: emerging mechanisms and functions. *Trends Cell Biol* 2024; 34: 771–784.
39. Kharel P, Fay M, Manasova EV, Anderson PJ, Kurkin AV, Guo JU *et al*. Stress promotes RNA G-quadruplex folding in human cells. *Nat Commun* 2023; 14: 205.
40. Biffi G, Di Antonio M, Tannahill D, Balasubramanian S. Visualization and selective chemical targeting of RNA G-quadruplex structures in the cytoplasm of human cells. *Nat Chem* 2014; 6: 75–80.
41. Paz I, Kosti I, Ares M, Cline M, Mandel-Gutfreund Y. RBPmap: a web server for mapping binding sites of RNA-binding proteins. *Nucleic Acids Res* 2014; 42: W361–W367.
42. Herviou P, Le Bras M, Dumas L, Hieblot C, Gilhodes J, Cioci G *et al*. hnRNP H/F drive RNA G-quadruplex-mediated translation linked to genomic instability and therapy resistance in glioblastoma. *Nature Communications* 2020; 11.
43. De Silva NIU, Lehman N, Fargason T, Paul T, Zhang ZH, Zhang J. Unearthing a novel function of SRSF1 in binding and unfolding of RNA G-quadruplexes. *Nucleic Acids Res* 2024; 52: 4676–4690.
44. Zahler AM, Lane WS, Stolk JA, Roth MB. Sr Proteins - a Conserved Family of Pre-Messenger-Rna Splicing Factors. *Gene Dev* 1992; 6: 837–847.

45. Cáceres JF, Screaton GR, Krainer AR. A specific subset of SR proteins shuttles continuously between the nucleus and the cytoplasm. *Gene Dev* 1998; 12: 55–66.
46. Cazalla D, Zhu J, Manche L, Huber E, Krainer AR, Cáceres JF. Nuclear export and retention signals in the RS domain of SR proteins. *Mol Cell Biol* 2002; 22: 6871–6882.
47. Twyffels L, Gueydan C, Kruys V. Shuttling SR proteins: more than splicing factors. *FEBS J* 2011; 278: 3246–3255.
48. Wagner RE, Frye M. Noncanonical functions of the serine-arginine-rich splicing factor (SR) family of proteins in development and disease. *Bioessays* 2021; 43: e2000242.
49. Ong SE, Mittler G, Mann M. Identifying and quantifying in vivo methylation sites by heavy methyl SILAC. *Nat Methods* 2004; 1: 119–126.
50. Sinha R, Allemand E, Zhang Z, Karni R, Myers MP, Krainer AR. Arginine methylation controls the subcellular localization and functions of the oncoprotein splicing factor SF2/ASF. *Mol Cell Biol* 2010; 30: 2762–2774.
51. Radzisheuskaya A, Shliaha PV, Grinev V, Lorenzini E, Kovalchuk S, Shlyueva D *et al*. PRMT5 methylome profiling uncovers a direct link to splicing regulation in acute myeloid leukemia. *Nat Struct Mol Biol* 2019; 26: 999–1012.
52. Li D, Yu W, Lai M. Towards understandings of serine/arginine-rich splicing factors. *Acta Pharm Sin B* 2023; 13: 3181–3207.
53. Das S, Krainer AR. Emerging functions of SRSF1, splicing factor and oncoprotein, in RNA metabolism and cancer. *Mol Cancer Res* 2014; 12: 1195–1204.
54. Tang S, Fang Y, Huang G, Xu X, Padilla-Banks E, Fan W *et al*. Methionine metabolism is essential for SIRT1-regulated mouse embryonic stem cell maintenance and embryonic development. *EMBO J* 2017; 36: 3175–3193.
55. Hardie DG, Ross FA, Hawley SA. AMPK: a nutrient and energy sensor that maintains energy homeostasis. *Nat Rev Mol Cell Biol* 2012; 13: 251–262.
56. Garcia D, Shaw RJ. AMPK: Mechanisms of Cellular Energy Sensing and Restoration of Metabolic Balance. *Mol Cell* 2017; 66: 789–800.
57. Sun K, Montana V, Chellappa K, Brelivet Y, Moras D, Maeda Y *et al*. Phosphorylation of a conserved serine in the deoxyribonucleic acid binding domain of nuclear receptors alters intracellular localization. *Mol Endocrinol* 2007; 21: 1297–1311.
58. Yu D, Chen G, Pan M, Zhang J, He W, Liu Y *et al*. High fat diet-induced oxidative stress blocks hepatocyte nuclear factor 4alpha and leads to hepatic steatosis in mice. *J Cell Physiol* 2018; 233: 4770–4782.
59. Garate-Rascon M, Recalde M, Jimenez M, Elizalde M, Azkona M, Uriarte I *et al*. Splicing Factor SLU7 Prevents Oxidative Stress-Mediated Hepatocyte Nuclear Factor 4alpha Degradation, Preserving Hepatic Differentiation and Protecting From Liver Damage. *Hepatology* 2021; 74: 2791–2807.
60. Matsumoto E, Akiyama K, Saito T, Matsumoto Y, Kobayashi KI, Inoue J *et al*. AMP-activated protein kinase regulates alternative pre-mRNA splicing by phosphorylation of SRSF1. *Biochem J* 2020; 477: 2237–2248.
61. Sun L, Sadighi Akha AA, Miller RA, Harper JM. Life-span extension in mice by preweaning food restriction and by methionine restriction in middle age. *J Gerontol A Biol Sci Med Sci* 2009; 64: 711–722.
62. Malloy VL, Perrone CE, Mattocks DA, Ables GP, Caliendo NS, Orentreich DS *et al*. Methionine restriction prevents the progression of hepatic steatosis in leptin-deficient obese mice. *Metabolism* 2013; 62: 1651–

1661.

63. Ables GP, Hens JR, Nichenametla SN. Methionine restriction beyond life-span extension. *Ann N Y Acad Sci* 2016; 1363: 68–79.
64. Ables GP, Johnson JE. Pleiotropic responses to methionine restriction. *Exp Gerontol* 2017; 94: 83–88.
65. Battle MA, Konopka G, Parviz F, Gaggl AL, Yang C, Sladek FM *et al*. Hepatocyte nuclear factor 4alpha orchestrates expression of cell adhesion proteins during the epithelial transformation of the developing liver. *Proc Natl Acad Sci U S A* 2006; 103: 8419–8424.
66. Santangelo L, Marchetti A, Cicchini C, Conigliaro A, Conti B, Mancone C *et al*. The stable repression of mesenchymal program is required for hepatocyte identity: a novel role for hepatocyte nuclear factor 4alpha. *Hepatology* 2011; 53: 2063–2074.
67. Lau HH, Ng NHJ, Loo LSW, Jasmen JB, Teo AKK. The molecular functions of hepatocyte nuclear factors - In and beyond the liver. *J Hepatol* 2018; 68: 1033–1048.
68. Guo S, Lu H. Conjunction of potential G-quadruplex and adjacent cis-elements in the 5' UTR of hepatocyte nuclear factor 4-alpha strongly inhibit protein expression. *Sci Rep* 2017; 7: 17444.
69. Trackman PC, Saxena D, Bais MV. TGF-beta1- and CCN2-Stimulated Sirius Red Assay for Collagen Accumulation in Cultured Cells. *Methods Mol Biol* 2017; 1489: 481–485.
70. Dobin A, Davis CA, Schlesinger F, Drenkow J, Zaleski C, Jha S *et al*. STAR: ultrafast universal RNA-seq aligner. *Bioinformatics* 2013; 29: 15–21.
71. Liao Y, Smyth GK, Shi W. The Subread aligner: fast, accurate and scalable read mapping by seed-and-vote. *Nucleic Acids Res* 2013; 41: e108.
72. Zhang Z, Kunwar P, Yu Y, Prevelige P, Zhang J. Phosphorylation-dependent regulation of serine/arginine-rich proteins and U2AF1 interactions in early spliceosome assembly. *J Biol Chem* 2026; 302: 111222.
73. Surani AA, Montiel-Duarte C. Native RNA G quadruplex immunoprecipitation (rG4IP) from mammalian cells. *STAR Protoc* 2022; 3: 101372.
74. Luige J, Armaos A, Tartaglia GG, Orom UAV. Predicting nuclear G-quadruplex RNA-binding proteins with roles in transcription and phase separation. *Nat Commun* 2024; 15: 2585.

Figures

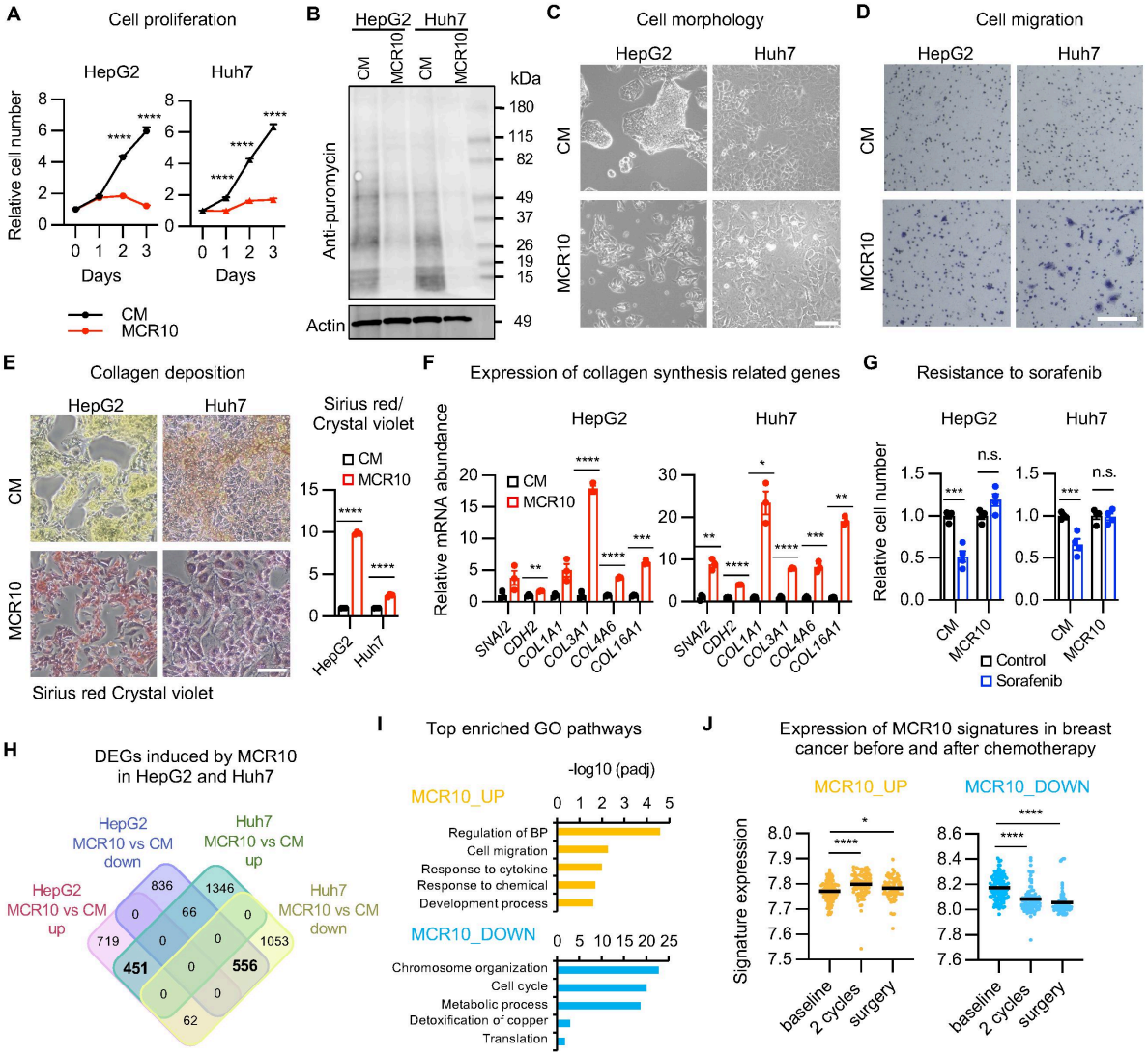


Figure 1

Characterization of MCR10 persisters in HCC.

(A) HepG2 and Huh7 MCR10 persisters exhibit reduced proliferation. The growth curves of parental HepG2 and Huh7 cells (cultured in CM) or MCR10 persisters (cultured in MCR10 medium) were quantified by the Cyquant assay (n=4 replicates/group, multiple 2-tailed unpaired Student's t-test, ****p<0.0001). (B) HepG2 and Huh7 MCR10 persisters display decreased protein synthesis. Puromycin incorporation into newly synthesized peptides was compared between MCR10 persisters and parental CM cells using the SUnSET assay. (C) Prolonged MCR10 treatment induces mesenchymal-like morphological changes. Parental HepG2 and Huh7 cells (CM) and MCR10 persisters (cultured in the MCR10 medium for 4 days). Bar, 100 mm. (D) MCR10 persisters display markedly enhanced migratory capacity. The migratory capacity of parental CM cells or MCR10 persisters was analyzed by the cell migration assay as described in Methods. Bar, 50 mm. (E) Collagen deposition is elevated in MCR10 persisters. The Collagen deposition levels of parental CM cells or MCR10 persisters was quantified by Sirius red staining as described in Methods (n=3 replicates/group, 2-tailed unpaired Student's t-test, ****p<0.0001). Bar, 50 mm. (F) Expression of EMT-associated genes is upregulated in MCR10 persisters. The mRNA levels of HNF4a targets and EMT related genes from parental CM cells or MCR10 persisters were quantified by qPCR (n=3

replicates/group, multiple 2-tailed unpaired Student's t-test, *p<0.05, **p<0.01, ***p<0.001, ****p<0.0001). (G) MCR10 persisters show increased resistance to sorafenib treatment, maintaining higher viable cell numbers relative to CM cells. Parental CM cells of MCR10 cells were treated with 10 mM of Sorafenib for 24 hours. The surviving cells numbers were quantified with the Cyquant assay (n=4 replicates/group, 2-tailed unpaired Student's t-test, ***p<0.001, n.s., not significant). (H) Venn diagram analysis of MCR10 altered protein-coding DEGs in HepG2 and Huh7 cells (|FC|≥2, FDR<0.05). Transcriptomic profiles of parental CM cells and MCR10 persisters were analyzed by RNA-seq. (I) Top enriched GO pathways in the commonly upregulated (MCR10_UP) or downregulated (MCR10_DOWN) genes highlighted in (A). Enrichment score represents $-\log_{10}$-transformed *p*-values after adjusted for FDR. (J) Expression of MCR10 signatures in breast cancer before and after chemotherapy. A publicly available RNA-seq dataset of breast cancer samples collected before treatment (baseline), after two cycles of chemotherapy (2 cycles), and at final surgery following six cycles of chemotherapy (surgery) [24] was analyzed for the expression of MCR10_UP signature and MCR10_DOWN signature (n=122, 82, and 71 patient samples, respectively; Brown-Forsythe and Welch ANOVA test adjusted for FDR, *q<0.05, ****q<0.0001).

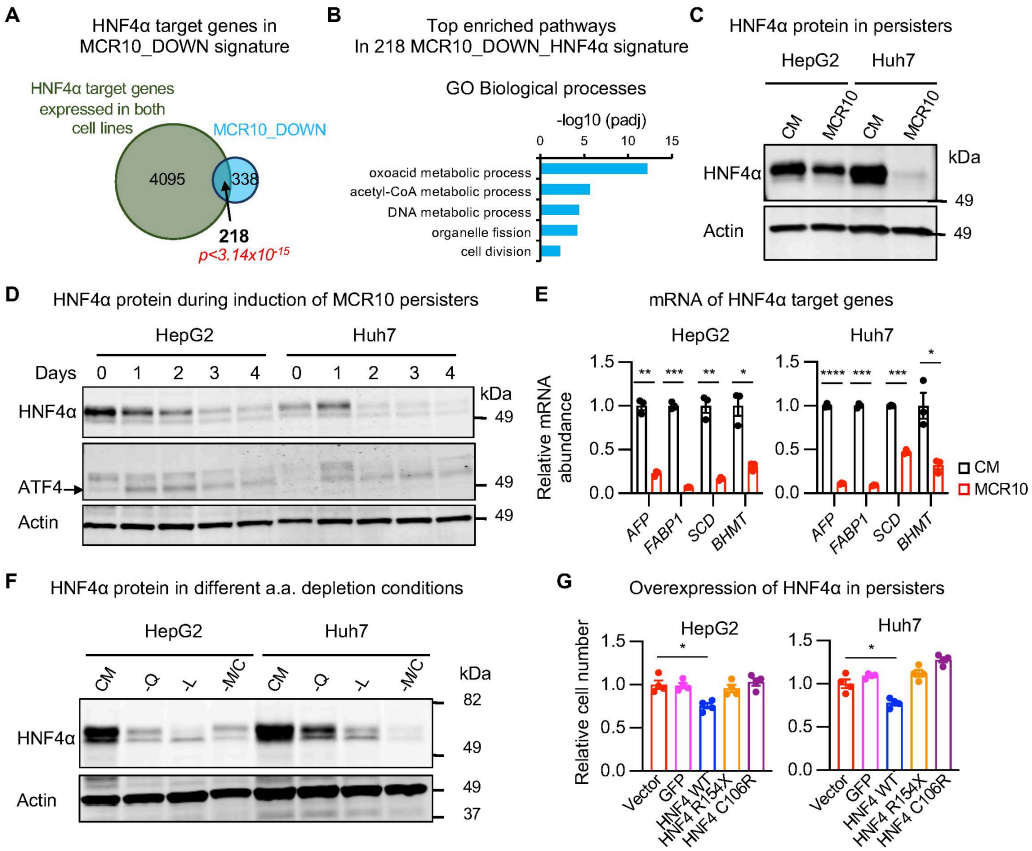


Figure 2

MCR10 persisters have reduced HNF4a protein and transcriptional activity.

(A) 218 out of the 556 downregulated Cluster 2 genes shared by HepG2 and Huh7 persister are HNF4a target genes. 4,313 protein coding HNF4a target genes with RPKM > 1 in both HepG2 and Huh7 cells in our RNA-seq dataset were identified out of 6,484 total HNF4a target genes reported in ChEA [28, 29] (https://maayanlab.cloud/Harmonizome/gene_set/HNF4A/CHEA+Transcription+Factor+Targets). The p value of gene overlap was determined using an exact hypergeometric probability test, with 17,664 total protein-coding genes in HepG2 and Huh7 cells as the background. (B) GO pathway analysis of 218 HNF4a targets downregulated by MCR10 targets highlights disrupted metabolism and cell division. Enrichment score represents $-\log_{10}$-transformed *p*-values after adjusted for FDR. (C) MCR10 persisters have reduced HNF4a protein abundance compared to parental CM cells. (D) HNF4a protein levels progressively decline during MCR10 treatment. Parental HepG2 or Huh7 cells were treated with MCR10 medium up to 4 days. (E) Multiple HNF4a target genes unrelated to mesenchymal morphology were significantly downregulated in MCR10 persisters. The mRNA levels of indicated genes were analyzed by qPCR (n=3 replicates/group, 2-tailed unpaired Student's t-test, *p<0.05, **p<0.01, ***p<0.001, and ****p<0.0001). (F) Reduced HNF4a protein levels following glutamine or leucine depletion. Cells were treated in CM (complete medium), -G (0.2 mM of L-glutamaine instead of 4 mM L-glutamaine in CM), -L (0.04 mM of leucine instead of 0.8 mM leucine in CM), -M/C (10 mM of methionine and 10 mM of cysteine instead of 200 mM of methionine and 200 mM of cysteine in CM) for 4 days. (G) Overexpression of WT but not mutant HNF4a protein partially restores the sensitivity of MCR10 persisters to MCR10 treatment. Constructs overexpressing WT, C106R, or R156X HNF4a, or GFP control were transfected into the MCR10 persisters. The cell numbers were quantified by crystal violet assay 24 hours later (n=4 replicates/group, Brown-Forsythe and Welch ANOVA test adjusted for FDR, *q<0.05).

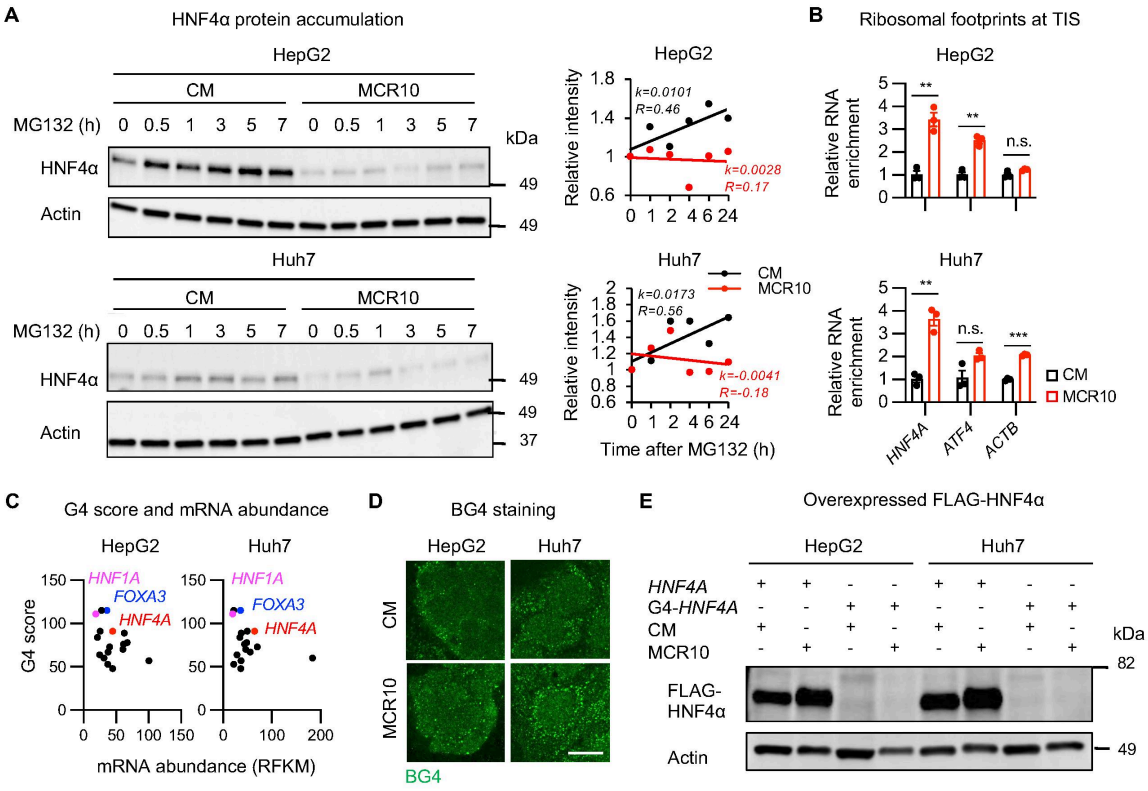


Figure 3

RNA G-quadruplex (rG4)-mediated translational suppression of HNF4a in MCR10 persisters.

(A) MG132 treatment increased HNF4a protein in parental cells, but not in MCR10 persisters. Parental CM cells or MCR10 persisters were treated with 10 mM MG132 up to 7 hrs. (B) Reduced ribosomal occupancy at the translation initiation site of *HNF4A* mRNA in MCR10 persisters. Targeted ribosomal footprinting was performed on cell lysates from parental CM cells and MCR10 persisters. Ribosome-protected fragments near translation start sites were quantified by qPCR following RNase digestion (n=3 replicates/group, multiple 2-tailed unpaired Student's t-test, **p<0.01, ***p<0.001, and n.s., not significant). (C) HNF4a is one of the most abundant transcription factors with high G4 scores in both HepG2 and Huh7 cells. (D) MCR10 persisters have increased cytosolic G4 staining intensity. Parental CM cells and MCR10 persisters were stained with a BG4 antibody that specifically recognizes and binds to G-quadruplex structures. Bar, 20 mm. (E) The endogenous *HNF4A* rG4 element strongly suppresses HNF4atranslation in a mammalian expression construct. FLAG-tagged HNF4aexpression constructs with (G4-*HNF4A*) or without (*HNF4A*) the endogenous *HNF4A* rG4 element at the 5'-UTR were transfected into parental HepG2 or Huh7 cells. Exogenous HNF4aprotein levels were detected using an anti-FLAG antibody.

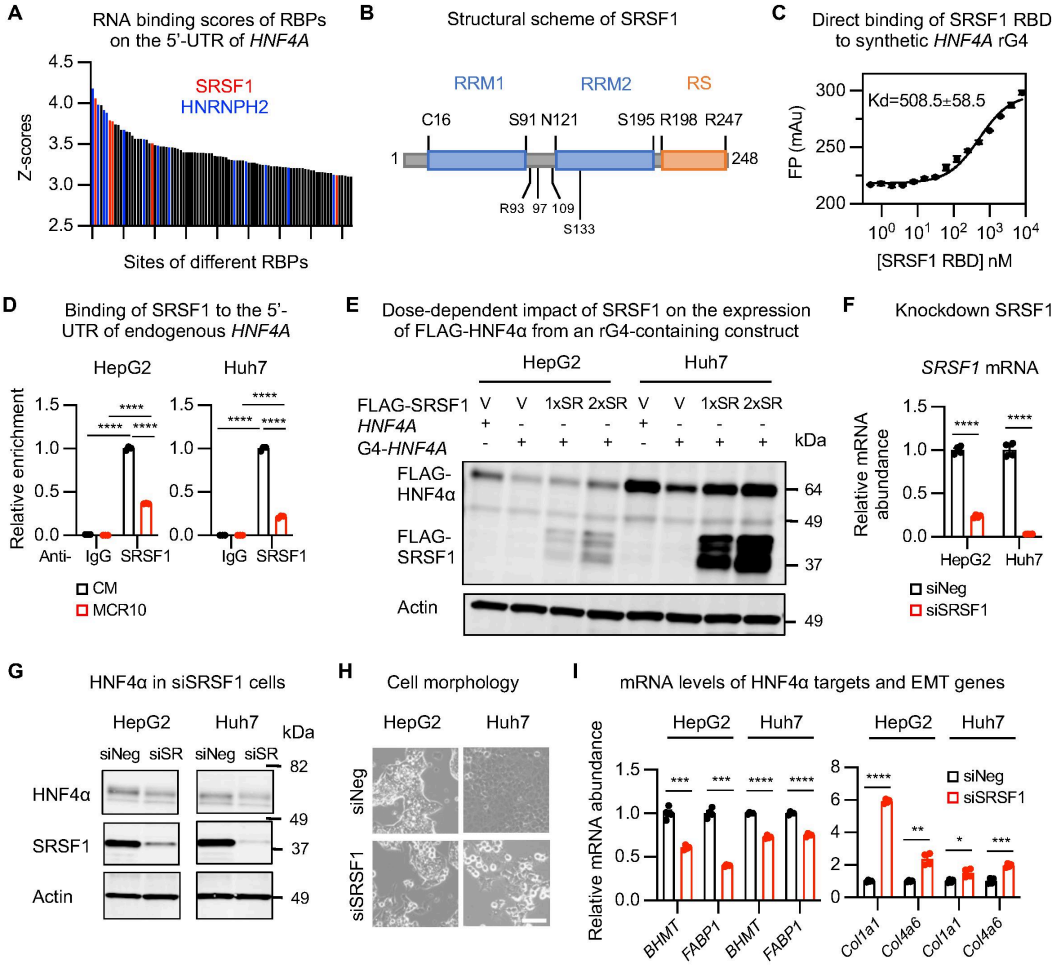


Figure 4

SRSF1 binds HNF4A rG4 and suppresses HNF4a expression in MCR10 persisters.

(A) SRSF1 has high predicted binding scores across multiple sites within the 5'-UTR of *HNF4A* gene. The potential RNA binding proteins (RBPs) interaction sites within the 5'-UTR of *HNF4A* gene were analyzed using RBPmap [41]. (B) The structural scheme of SRSF1. SRSF1 contains two N-terminal RRMs and a C-terminal RS domain. (C) The SRSF1 RNA-binding domain directly binds to the *HNF4A*rG4 element in vitro with a Kd of ~500 nM (n=3 replicates). (D) MCR10 persisters have reduced binding of SRSF1 to the 5'-UTR of *HNF4A*. Toal cell lysates from parental CM cells and MCR10 persisters were immunoprecipitated with anti-SRSF1 antibodies, and the associated RNA extracted and analyzed by qPCR (n=3 replicates/group, 2-way ANOVA adjusted for FDR, ****q<0.0001). (E) SRSF1 dose-dependently increases HNF4a translation from an rG4-containing construct. Parental HepG2 and Huh7 CM cells were co-transfected with FLAG-tagged rG4-containing HNF4A constructs (G4-HNF4A) and two doses of FLAG-tagged SRSF1 plasmids (2×SR containing twice the DNA amount of 1×SR), and overexpressed HNF4a and SRSF1 proteins were analyzed using an anti-FLAG antibody. (F-G) siRNA-mediated SRSF1 knockdown reduces the abundance of endogenous HNF4a protein. Negative control siRNA (siNeg) or siRNAs against SRSF1 (siSRSF1) were transfected into parental HepG2 and Huh7 CM cells with

Lipofectamine RNAiMAX. (F) The mRNA levels of SRSF1 were quantified by qPCR (n=4 replicates/group, 2-tailed unpaired Student's t-test, ****p<0.0001). (G) The protein levels of SRSF1 and HNF4a were analyzed by immunoblotting. (H) SRSF1 knockdown induces a mesenchymal-like morphology in parental CM cells. Parental HepG2 and Huh7 CM cells were transfected with a negative control siRNA or siSRSF1. The cell morphology was analyzed 48 hours later. Bar, 100 mm. (I) SRSF1 knockdown reduces the expression of HNF4a target genes while increasing EMT-related gene expression. Parental HepG2 and Huh7 CM cells transfected with a negative control siRNA or siSRSF1 were analyzed for the expression of indicated genes 48 hours later by qPCR (n=3 replicates/group, multiple 2-tailed unpaired Student's t-test, *p<0.05, **p<0.01, ***p<0.001, ****p<0.0001).

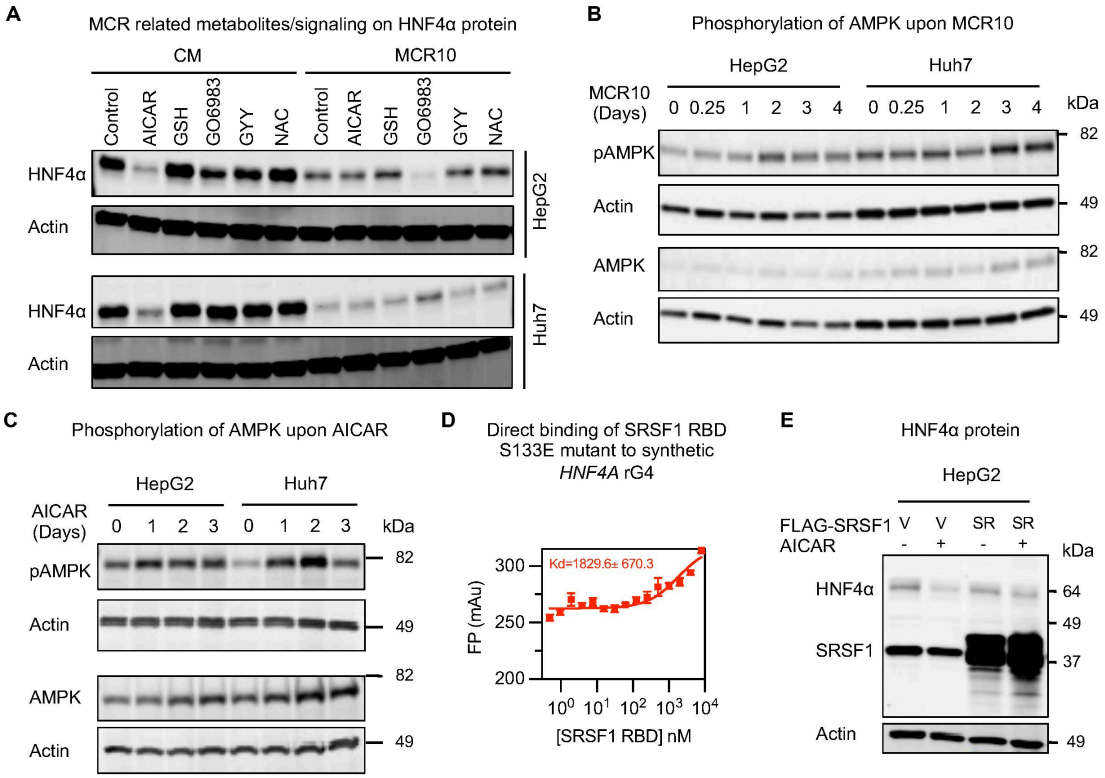


Figure 5

Activation of AMPK suppresses HNF4aexpression.

(A) AICAR mimics MCR10 to suppress the expression of HNF4a protein. Parental cells and MCR10 persisters were treated with 500 μM AICAR, 1.5 mM GSH, 5 μM GO6983, 500 μM GYY4137 (GYY), or 1.2 mM NAC for 4 days. (B) The phosphorylation of AMPK is increased during induction of MCR10 persisters. Parental HepG2 or Huh7 cells were cultured with MCR10 medium up to 4 days. The abundance of total AMPK and pAMPK was

analyzed by immunoblotting. (C) AICAR treatment induces phosphorylation of AMPK. Cell cultured in CM were treated with 500 μM AICAR for indicated days. (D) The phosphomimetic SRSF1 RBD S133E mutant exhibited reduced binding affinity for the *HNF4A* rG4 element in vitro, with a Kd of approximately 1,800 nM (n=6 replicates). (E) SRSF1 overexpression partially restores HNF4a abundance after AICAR treatment. Parental HepG2 CM cells transfected with Flag-SRSF1 (SR) were treated with 500 mM AICAR for 48 hours. The endogenous HNF4a protein was analyzed by immunoblotting.

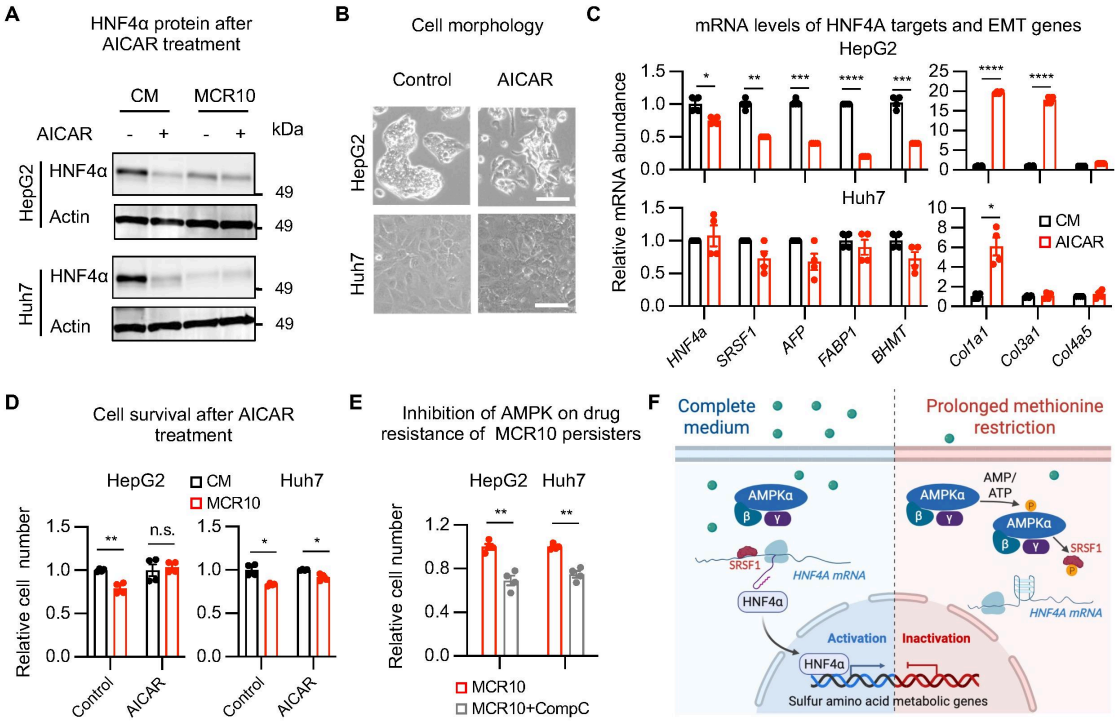


Figure 6

The AMPK–SRSF1 axis mediates HNF4a suppression and drug tolerance in MCR10 persisters.

(A) AICAR treatment reduced the abundance of HNF4a protein. Parental HepG2 or Huh7 CM cells or MCR10 persisters were treated with or without 500 mM AICAR for 4 days. (B) AICAR induces mesenchymal-like morphology. Parental HepG2 and Huh7 CM cells were treated with 500 mM AICAR for 4 days. Bars, 100 mm. (C) AICAR reduces the expression of HNF4α target genes and increases the levels of EMT genes. Parental HepG2 and Huh7 CM cells were treated with 500 mM AICAR for 4 days. The mRNA levels of HNF4a targets and EMT related genes were quantified by qPCR (n=4 replicates/group, multiple 2-tailed unpaired Student's t-test, *p<0.05,

**p<0.01, ***p<0.001, ****p<0.0001). (D) AICAR-treated cells are resistant to MCR10-induced inhibition of cell growth. Parental HepG2 and Huh7 CM cells were treated with or without 500 mM AICAR for 4 days. The remaining cells were subjected to further treatment with MCR10 medium for 24 hours. The cells numbers were then quantified with the Cyquant assay (n=4 replicates/group, multiple 2-tailed unpaired Student's t-test, *p<0.05, **p<0.01, n.s., not significant). (E) Inhibition of AMPK by compound C sensitizes MCR10 persisters to MCR10 treatment. HepG2 or Huh7 MCR10 persisters were cultured in either MCR10 medium only or MCR10 medium containing 10 mM compound C for 24 hours. The cell numbers were then quantified using the crystal violet assay (n=4 replicates/group, multiple 2-tailed unpaired Student's t-test, **p<0.01). (F) A working model depicting the mechanism underlying prolonged methionine restriction-induced persister cell formation in liver cancer cells. Under prolonged methionine restriction, AMPK activation leads to SRSF1 phosphorylation, reduced binding to the *HNF4A* rG4 element, suppression of HNF4a protein translation, and ultimately persister cell formation.

Supplementary Files

This is a list of supplementary files associated with this preprint. Click to download.

- TableS5primersequences.xlsx
- TableS4antibodies.xlsx
- TableS1RNAseqheatmapandvenndiagramanalysis.xlsx
- Xuetal.FigureSs62526.pdf
- TableS2HNF4aControlvsKDmicroarray.xlsx
- TableS3218MRreducedHNF4Atargetsv2.xlsx